Relating Satellite-Observed Cloud Properties from MODIS to Meteorological Conditions for Marine Boundary Layer Clouds

GUANG J. ZHANG

Scripps Institution of Oceanography, La Jolla, California

ANDREW M. VOGELMANN AND MICHAEL P. JENSEN

Brookhaven National Laboratory, Upton, New York

WILLIAM D. COLLINS

Department of Earth and Planetary Science, University of California, Berkeley, and Earth Sciences Division, Lawrence Berkeley National Laboratory, Berkeley, California

EDWARD P. LUKE

Brookhaven National Laboratory, Upton, New York

(Manuscript received 20 October 2008, in final form 9 October 2009)

ABSTRACT

This study examines 6 yr of cloud properties observed by the Moderate Resolution Imaging Spectroradiometer (MODIS) on board the NASA *Terra* satellite in five prominent marine boundary layer (MBL) cloud regions (California, Peru, Canary, Angola, and Australia) and investigates their relationships with near-surface meteorological parameters obtained from NCEP reanalyses. About 62 000 independent scenes are used to examine the instantaneous relationships between cloud properties and meteorological parameters that may be used for global climate model (GCM) diagnostics and parameterization. Cloud liquid water path (LWP) generally increases with lower-tropospheric stability (LTS) and lifting condensation level (LCL), whereas cloud drizzle frequency is favored by weak LTS and negligible cold air advection. Cloud fraction (CF) depends strongly on variations in LTS, and to a lesser extent on surface air temperature advection and LCL, although the relationships vary from region to region. The authors propose capturing the effects of these three parameters on CF via their linear combination in terms of a single parameter, the effective lower-tropospheric stability (eLTS). Results indicate that eLTS offers a marked improvement over LTS alone in explaining the median CF variations within the different study regions. A parameterization of CF in terms of eLTS is provided, which produces results that are improved over those of Klein and Hartmann's LTS-only parameterization. However, the new parameterization may not predict the observed variability correctly, and the authors propose a method that might address this shortcoming via a statistical approach.

1. Introduction

Marine boundary layer (MBL) clouds have a strong shortwave cloud radiative forcing on the earth's climate system (Klein and Hartmann 1993). They form in the cold water regions off the west coast of major continents; via strong radiative cooling, they play an important role in modulating the sea surface temperatures (SSTs). However, their simulation in global climate models (GCMs) is among the most problematic, and few models can simulate the extent of these clouds (Ma et al. 1996; Siebesma et al. 2004) or their albedos realistically (Zhang et al. 2005; Bender et al. 2006). Resolving these shortcomings is particularly important for climate change studies because of the importance of the MBL clouds in the global radiation budget.

For these reasons, representation of these clouds in terms of the large-scale meteorological parameters in GCMs has been an active research subject through observational and theoretical studies. Surface and satellite

Corresponding author address: Guang J. Zhang, Scripps Institution of Oceanography, La Jolla, CA 92093-0221.
E-mail: gzhang@ucsd.edu

DOI: 10.1175/2009JCLI2897.1

observations show that the amount of low-level marine clouds is highly correlated with lower-tropospheric stability (LTS), which is defined as the potential temperature difference between 700 and 1000 mb; SST; and cold air advection on subseasonal to interannual time scales (Wylie et al. 1989; Klein and Hartmann 1993; Norris and Leovy 1994; Klein et al. 1995; Philander et al. 1996; Xu et al. 2005; Wood and Hartmann 2006; Mochizuki et al. 2007). Klein and Hartmann (1993) show that surface-observed cloud fraction (CF) is highly correlated with LTS on seasonal to interannual time scales, where CF increases by 5.7% for each 1 K increase in LTS. Klein et al. (1995) further investigate the relationships among marine CF, SST, and atmospheric circulation using 25 yr of observations from an ocean weather station in the northeastern Pacific. They find that cloud amount is well correlated with SSTs that are upstream of the trade winds blowing through the observation site. GCMs often incorporate in some fashion the observed relationships between the meteorological parameters and CF. For instance, the National Center for Atmospheric Research (NCAR) Community Atmosphere Model, version 3 (CAM3; Collins et al. 2004) parameterizes the MBL CF on the basis of the observed relationship between LTS and CF by Klein and Hartmann (1993). However, Dai and Trenberth (2004) find that such an LTS–cloud cover parameterization, based on seasonally averaged data, systematically underestimates the MBL CF.

These studies focused on large spatial scales that are commensurate with the sizes of GCM grid cells (e.g., 300 km $\times$ 300 km); however, we should note that a recent subject of intense research has been the spatial and temporal variability of mesoscale structures that are subgrid scale but have important consequences at large scales. Of particular interest are pockets of open cells (POCs; Stevens et al. 2005) that are embedded in otherwise uniform stratocumulus and resemble broad regions of open mesoscale cellular convection (MCC). POCs and open MCCs are long lived and contain amounts of drizzle that are substantially larger than the smaller amounts found in the surrounding unbroken, stratiform clouds (Comstock et al. 2007); in fact, recent research has indicated that the occurrence of drizzle may play a key role in forming and sustaining the observed structures (Wood et al. 2008). Wood and Hartmann (2006) find that MCCs are strongly associated with the spatial variability of liquid water path (LWP) and CF in the marine stratocumulus regions off the Californian and Peruvian coasts. Although they find that open MCCs tend to locate downstream from closed MCCs, the type of MCC is not found to be very sensitive to the large-scale meteorological state.

In this study, we investigate the MBL cloud properties obtained from the Moderate Resolution Imaging Spectroradiometer (MODIS) instrument on board the National Aeronautics and Space Administration (NASA) *Terra* satellite over different regions of the globe and attempt to relate them to prevailing near-surface meteorological conditions. Recently, Jensen et al. (2008) used a similar set of multiyear observations to quantify the long-term microphysical and macroscale characteristics of MBL clouds and their regional and seasonal variations. Because the present study is a follow-up of the Jensen et al. work, their major findings are summarized here to serve as background information. Using MODIS observations, tens of thousands of independent MBL cloud scenes of size 300 km $\times$ 300 km were selected over each of the five regions where MBL clouds are common (viz., the west coasts of Angola, Australia, California, Canary Islands, and Peru). All scenes were screened to minimize the potential contamination by other cloud types (among other possible sources of error) and cloud property statistics were compiled from the selected scenes. The mesoscale structure of these clouds was quantified using effective cloud diameter C_D, which measures the bulk cloud organization and provides information additional to CF as to how the cloud elements are organized at the mesoscale level within the scene. They find that although MBL clouds are often considered plane parallel, overcast clouds occur in only about 25% of the scenes. Examination of seasonal variation finds that the greatest mesoscale organization (largest values of C_D) tends to occur during the months of peak cloud occurrence. The frequency of drizzle occurrence is a minimum during the months of peak MBL cloud occurrence and a maximum during the off-peak months. The patterns of drizzle frequency as a function of C_D are different between peak and off-peak months, and they also vary from region to region. Finally, cloud LWP and visible optical depth trend strongly with C_D, with the greatest values occurring for the drizzling scenes; however, there are considerable interregional differences in the trends.

As a follow-up to Jensen et al. (2008), this study uses the individual cloud scenes to analyze the instantaneous cloud–meteorological relationships for cloud fraction (CF), cloud diameter C_D, cloud LWP and scene-wide drizzle occurrence. This leads to a modified parameterization of CF based on meteorological parameters and a suggestion for a method that treats the remaining unrepresented variance. The paper is organized as follows: Section 2 presents the data and analysis methods. Section 3 presents the results, which document the cloud properties, their relationships with meteorological conditions, and a parameterization based on the relationships. Section 4 summarizes the findings and concludes the paper.

2. Data and analysis methods

Figure 1 shows the regions used in this study, which were selected based on the surface cloud climatology study of Klein and Hartmann (1993) and Norris and Leovy (1994). They are referred to here as the Californian, Peruvian, Canarian, Angolan, and Australian regions. As described later, in each region satellite data and meteorological reanalyses are collocated for cloud scenes that are 300 km × 300 km, which is the approximate size of the grid cell used by GCMs for long-term climate simulations.

The 1-km-resolution MODIS observations on the NASA *Terra* sun-synchronous satellite are the source of cloud properties for this study. The cloud scene selection uses version 4 of the MODIS instantaneous pixel-level cloud product retrievals (MOD06_L2). *Terra* has an equatorial overpass at approximately the same local time (LT) daily in the ascending node (~2230 LT) and in the descending node (~1030 LT). Only the data from the 1030 LT overpass are used, because the MODIS retrievals we use require solar illumination. Six full years of data from March 2000 to February 2006 are analyzed. The MODIS cloud products include cloud optical thickness and near-cloud-top effective radius of cloud droplets, from which cloud LWP is derived using the formula (Wood and Hartmann 2006)

$$\mathrm{LWP} = \frac{5}{9}\rho_w \tau r_e, \tag{1}$$

which takes into account the typical increase of liquid water content with height in MBL clouds in terms of the density of water ρ_w, cloud optical depth τ, and effective cloud droplet radius r_e. Details of the MODIS cloud products are described in Platnick et al. (2003) and King et al. (2003).

The 1-km-resolution MODIS cloud products have been screened and quality-controlled extensively (Jensen et al. 2008). For each overpass, independent 300 km × 300 km sized scenes are identified using an automated cloud screening method detailed in Jensen et al. (2008). Because MBL clouds are our focus, special care was taken in data quality control to remove scenes contaminated by the presence of frontal clouds, deep convective clouds, sunglint, or other possible error sources. Jensen et al. (2008) limited the selection of cloud scenes to have CFs >20%. However, this study aims to determine possible relationships between cloud properties and prevailing meteorological conditions; should the same criteria be used, our results would be biased toward high CF regimes. To avoid such biases, we include cloud scenes with fractional cloud cover <20% in our analysis. This increases the sample size significantly, by about 25%

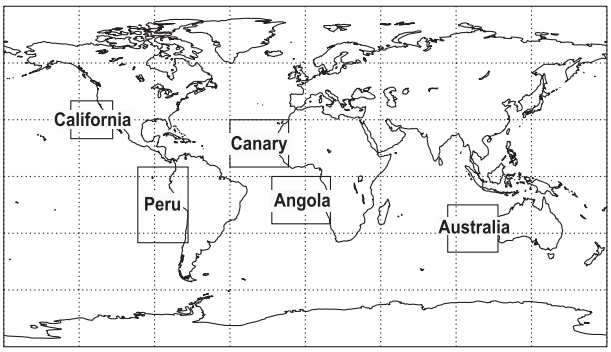

FIG. 1. Five MBL cloud regions. Each box indicates the location of a major MBL cloud region, based on the surface-based climatologies in Klein and Hartmann (1993) and Norris and Leovy (1994): from Jensen et al. (2008).

in high cloud cover regions (Angola, California, and Peru) and more than a factor of 2 in low cloud cover regions (Canary Islands and Australia), resulting in a total number of scenes close to 62 000. The cloud properties examined here include the scene CF and the in-cloud averages of LWP and r_e. Because of potential uncertainties in satellite retrievals of cloud properties at the edge of clouds, a binary cloud mask was used to locate pixels that are within three pixels from cloud edge and exclude them from the averages (however, they are not excluded for determinations of CF or effective cloud diameter, discussed next).

In addition, cloud size, as measured by the effective cloud diameter, is derived from each 300 km × 300 km cloud scene (for details, see Jensen et al. 2008). The average diameter of the clouds within the scene provides a bulk measure of how the marine boundary layer clouds are organized within a scene. Note that CF is a relative measure of the amount of cloud present within a scene of chosen size (or model grid box, in the case of a model), but C_D is mostly independent of model resolution or scene size. Although it would be desirable to be able to relate cloud diameter to the mesoscale variability attributed to open and closed MCCs (e.g., Wood and Hartmann 2006), ranges of cloud diameters do not directly correlate with their categories, because they use additional information about the LWP spatial structure that is not considered in our classification. The most that can be said is that smaller cloud diameters will contain open MCC (among other scattered cloud types) and intermediate values will contain closed MCCs.

Here, a cloud scene is characterized as containing significant drizzling clouds or not, based on a threshold applied to the scene-mean cloud particle effective radii r_e (for a more detailed discussion of the use of this drizzle threshold, see Jensen et al. 2008). Consistent with several previous studies (Pinsky and Khain 2002; Masunaga et al.

2002; Shao and Liu 2004), we classify a scene as containing significant drizzling clouds when $r_e \geq 15\ \mu$m (note that our scene-mean r_e is computed after removing the three rings of pixels at the cloud edge, which minimizes the likelihood of 3D effects or partially filled cloud pixels affecting the cloud property retrievals). We recognize that this threshold is somewhat crude and will not capture finer details of drizzle occurrence (such as drizzle rate) and will not be able to detect drizzle if it occurs at the base of a thick cloud. Although crude, comparisons with estimates from the more detailed parameterization of Bennartz (2007) found that only 11% of the scenes are identified differently. We remained with the 15-μm threshold because of its simplicity and the lack of additional data for the scenes required in the Bennartz parameterization. Thus, although it is possible that the drizzle occurrence for an individual scene could be misclassified, this approach is adequate for the purposes of surveying the bulk, long-term statistics between drizzle and meteorological state, particularly in light of the general lack of information on drizzle occurrence over large regions for seasonal and multiannual periods.

For meteorological data, we use the four times daily National Center for Environmental Predictions (NCEP)–NCAR reanalysis data (Kistler et al. 2001; available online at ftp://ftp.cdc.noaa.gov/Datasets/ncep.reanalysis). Based on a July study of a stratocumulus region off the Californian coast (Stevens et al. 2007), these reanalyses provide good averages of several meteorological state properties used here, with the exception of a slight warm bias at 850 mb. Because the *Terra* overpass is ~1030 LT, the reanalysis data from the two times that sandwich the *Terra* overpass are interpolated in time. For horizontal collocation of the NCEP–NCAR reanalysis data with the MODIS data, bilinear interpolation is used. The latitude and longitude of the center and four corners of each scene identify its location. The values of the meteorological variables at each of the five points are interpolated bilinearly from the 2.5° × 2.5° NCEP–NCAR reanalysis grid points. The scene average value is obtained using the following weighted average:

$$\overline{\chi} = \frac{1}{2}\left[\chi_c + \frac{1}{4}(\chi_1 + \chi_2 + \chi_3 + \chi_4)\right], \qquad (2)$$

where χ is any meteorological field, subscript c denotes the central point, and the subscript numbers denote the four corners. To analyze geographical distributions within each regional domain, the collocated satellite observation and reanalysis for each scene are mapped onto a 2.5° × 2.5° mesh. The long-term, representative values for each grid within the mesh are then obtained from medians of the cloud and meteorological properties.

We note that the MODIS data used here observe the diurnal variation of the MBL cloud state at a similar midmorning local time each day (1030 LT) and thus do not sample the diurnal variation. MBL clouds are influenced by boundary layer mixing and cloud-top entrainment, which are driven by the differential solar heating and infrared cooling at cloud top (e.g., as summarized in Comstock et al. 2005). At nighttime, infrared cooling causes air parcels to sink and mix in the MBL, as well as entrain drier air aloft at cloud top. This tends to thicken the cloud and increase the cloud cover. During daytime, solar radiation heats the cloud top and reduces the effects of infrared cooling, thereby reducing the cloud cover. We note that our results capture the midmorning state of this broad conceptual view of the diurnal cycle, which is generally a transition period between maximum and minimum cloud cover (Dai and Trenberth 2004); thus, these results may be indicative of the long-term mean. Furthermore, the variability of MBL cloud properties has been shown to be dominated by seasonal to annual time scales (Rozendaal and Rossow 2003), whereas daily to monthly time scales have smaller but nonnegligible variability. Thus, we expect our relationships, which are obtained based on instantaneous cloud scenes, to capture the dominant mode of variability, even though they cannot address diurnal variations.

3. Results

In this section, the general geographical distributions are discussed as background for the cloud properties (section 3a) and meteorological parameters (section 3b) before we discuss their instantaneous relationships. This sets the stage for section 3c, which uses this information to formulate and test a CF parameterization.

a. CF, effective cloud diameter, and liquid water path

Using the cloud scenes identified, we make 6 yr-regional composites of the median values of the scene CFs. Because the Jensen et al. (2008) selection criteria seek optimal MBL cloud scenes by minimizing potential contamination by other clouds or other artifacts, the scenes selected should be thought of as a representative sampling rather than a climatology. Figure 2 shows the six-year medians of CF for the regions given in Fig. 1. All regions have significant amount of clouds and region-to-region variability. The maximum CF exceeds 0.8 over large areas in the Californian, Peruvian, and Angolan regions, wheras the Canarian region has the smallest CF. The Australian region has a large amount of variability, with the MBL CF varying from <0.4 in the north to >0.8 in the south. These interregional differences are qualitatively similar

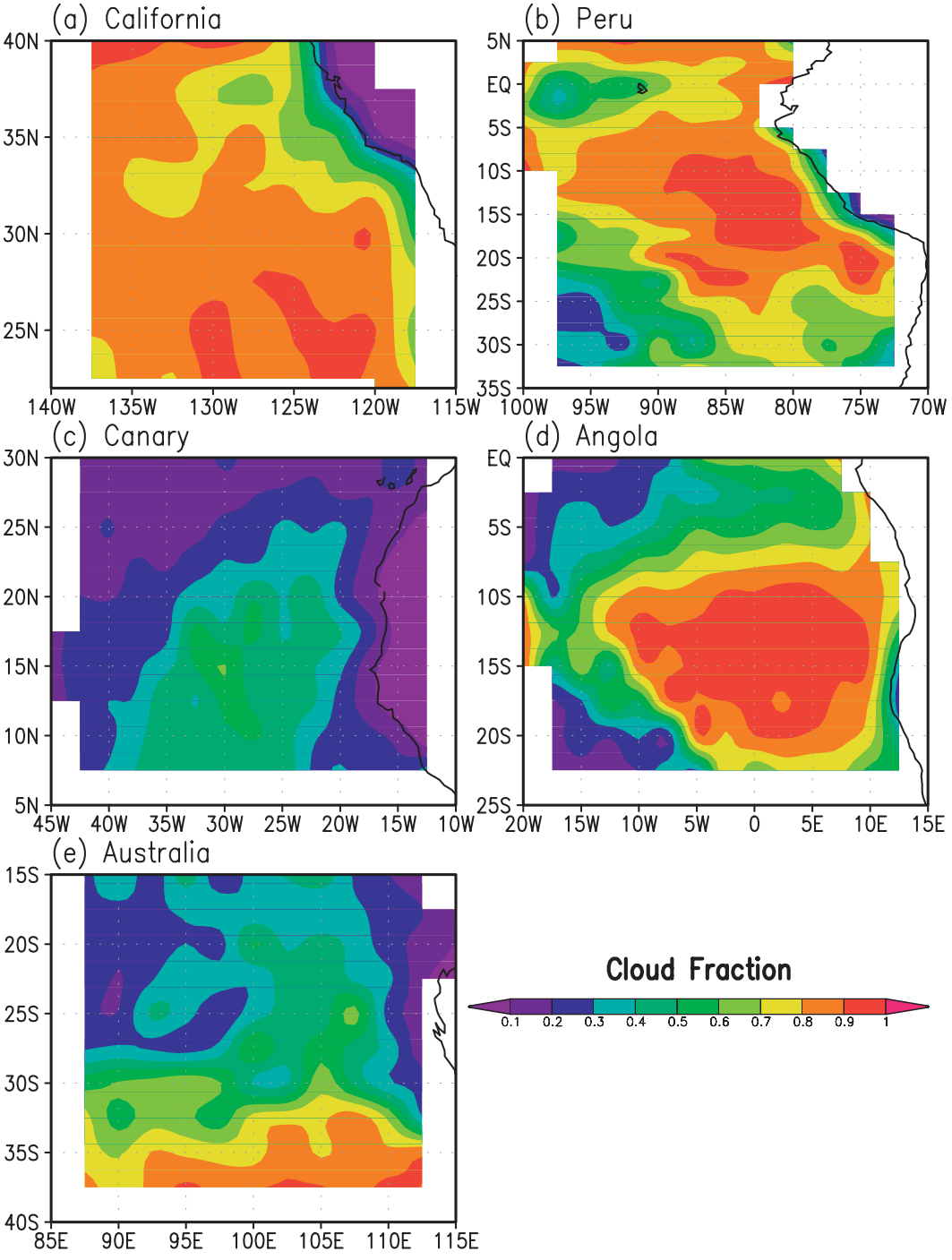

FIG. 2. CF distribution in the five MBL cloud regions (shown in Fig. 1) for 6 yr of data, based on all 300 km × 300 km cloud scenes identified in Jensen et al. (2008). The identification criteria they use seek optimal MBL cloud scenes, so the scenes selected should be thought of as a representative sampling rather than a climatology.

to those from surface observations climatology (Klein and Hartmann 1993).

The geographical patterns for C_D are similar to those found for CF (not shown). Cloud diameter is not diagnosed within GCMs; however, its average properties can be related to CF. Figure 3 shows the relationship between binned CF and C_D. For very large and very small clouds, CF varies only weakly with C_D; thus, in these regions, C_D provides additional sensitivity relative to CF on how the CF is distributed over the scene (Jensen et al.

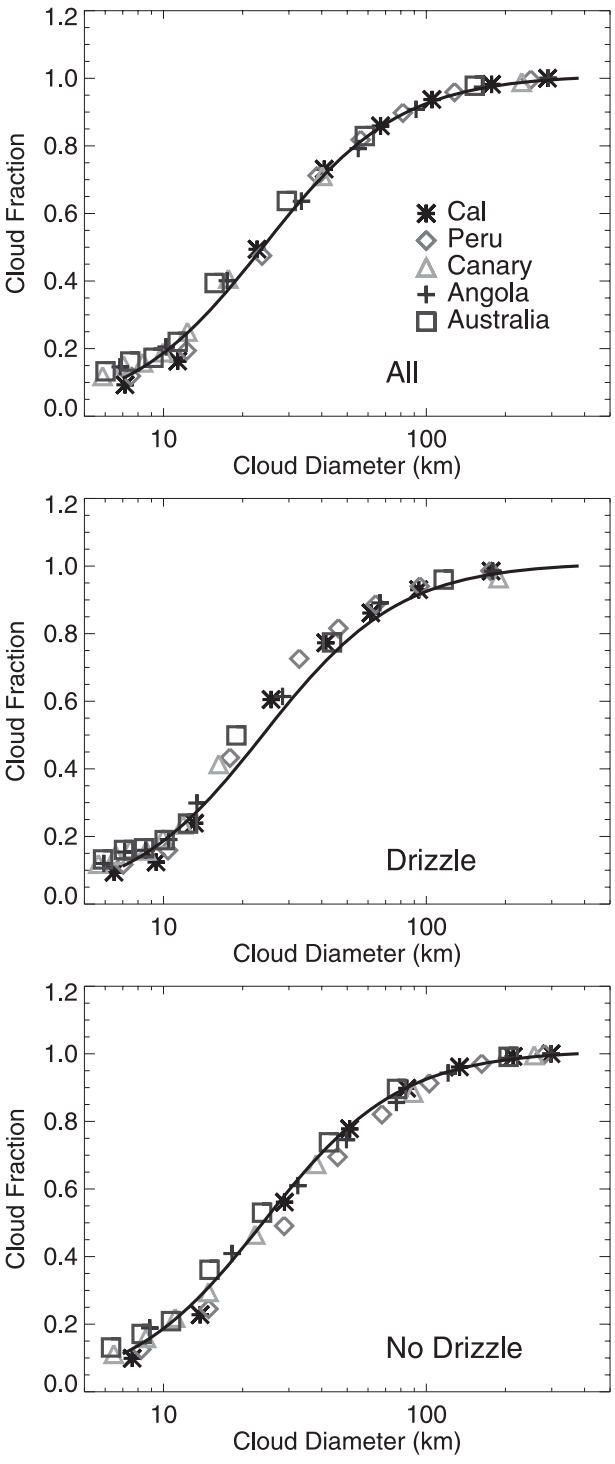

FIG. 3. Relationship between CF and C_D. Cloud diameter binning is determined for each region after sorting by C_D and dividing into eight equal-number bins. The median CF in each bin is plotted against the median C_D. All cloud scenes are included in the top frame, and only drizzling and nondrizzling cloud scenes are used in the middle and bottom frames, respectively. The sigmoidal fitting curve, generated from all data as described in the text, is plotted in all frames for reference.

2008). For medium-sized clouds (10–60 km in diameter), CF varies almost linearly with the logarithm of C_D. Also shown in the figure is a curve fit produced similarly to that in Jensen et al. (2008), which now includes the full range of available CF (versus having a 20% lower limit). The new fit is

$$y = \frac{a_0}{1 + e^{a_1 \ln C_d + a_2}}, \tag{3}$$

where y is CF and the fitting constants a_0, a_1, and a_2 are 1.01, 1.68, and 5.35, respectively. The functional form is the same as in Jensen et al. (2008), only the fitting constants are different.

Because the presence or absence of drizzle is an important characteristic of MBL clouds, we also plot the CF versus C_D relationship delimited by drizzle (Fig. 3). The fitted curve from all cloud scenes (Fig. 3a) is superposed for reference. The shapes of the drizzle and nondrizzle relationships are similar. Most of the points fall to the left of the curve for drizzling clouds and to the right for nondrizzling clouds, implying that, for a given CF, drizzling clouds are smaller than nondrizzling clouds. This is consistent with the observations that open cells are associated with drizzle (Comstock et al. 2007).

Figure 4 shows the spatial distributions of the cloud LWP per region. High LWP values are most common in the Peruvian region, with maximum values exceeding 100 g m^{-2}, whereas the Canarian region has the lowest LWP among all regions, varying from under 20 g m^{-2} off the coast of Senegal to 40 g m^{-2} in the open ocean. High LWP values in Peruvian region may explain why POCs form there frequently (Wood et al. 2008). Generally, LWP increases away from the coastline in all regions; for example, an east–west gradient is particularly apparent in the Californian region. Comparing these LWP fields with the CF (Fig. 2) shows that high LWP values often correlate with high CF (e.g., Peru, Australia, and Angola); however, exceptions from this general rule exist. For example, the Angolan LWP maximum is centered about 5° west from the CF maximum; similarly, the LWP maxima for the Californian and Canarian regions are mostly west of their CF maxima.

b. Relationships with meteorological conditions

MBL clouds tend to occur under certain meteorological conditions. Previous observations indicate that they often occur in subsidence regions with cold temperature advection and stable stratification (Klein and Hartmann 1993; Klein et al. 1995; Wylie et al. 1989; Xu et al. 2005; Wood and Hartmann 2006). In this subsection, we attempt to relate the cloud properties to prevailing near-surface meteorological conditions. A number of meteorological properties obtained from the NCEP reanalysis

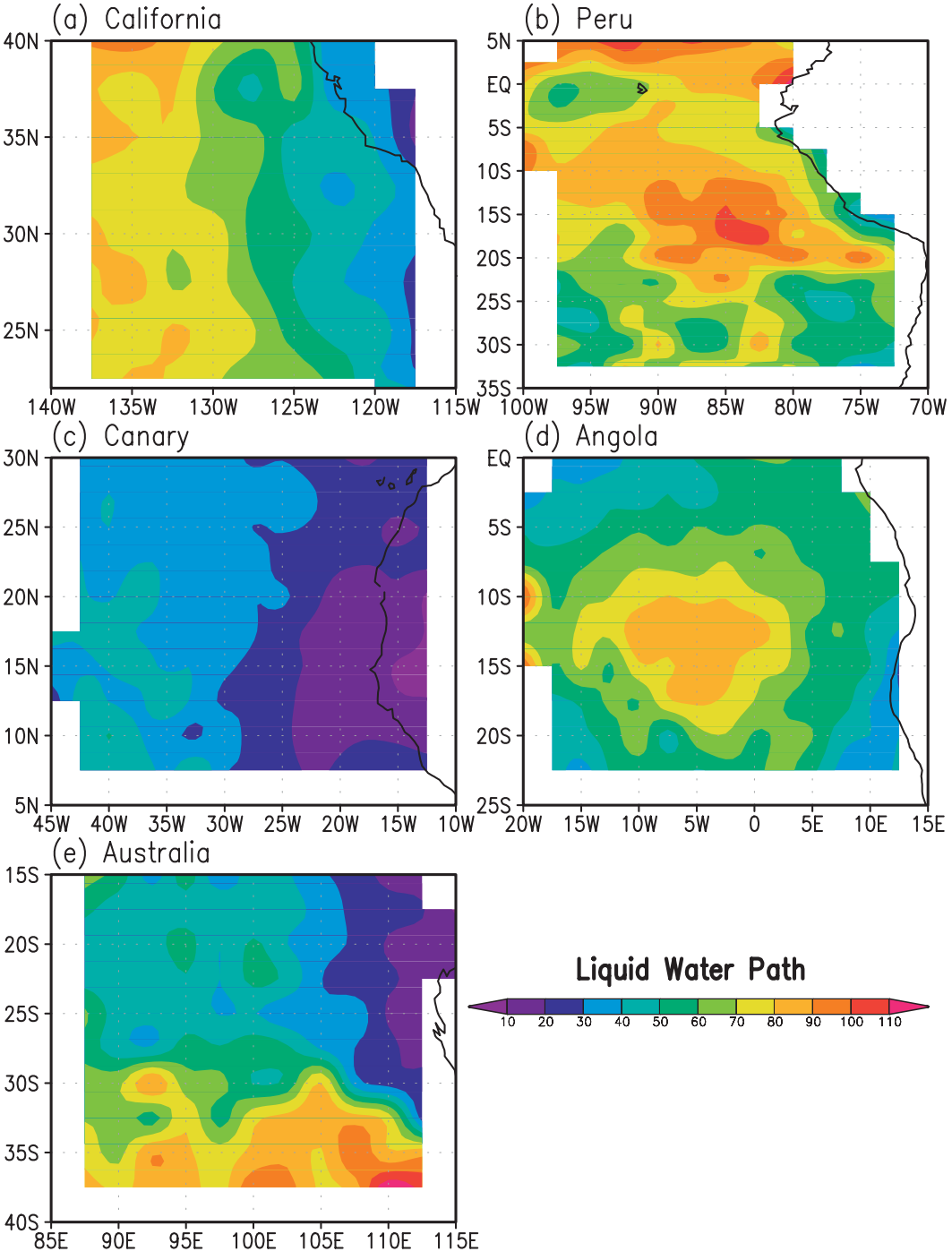

FIG. 4. As in Fig. 2, but for LWP distributions (g m^{-2}).

are examined extensively; they include 850-mb vertical velocity, LTS between 1000 and 700 mb, surface air temperature advection (advT), surface air moisture given by the lifting condensation level (LCL) of the near-surface (1000 mb) air, relative humidity (RH) at 850 mb, and the geopotential height and winds of the 850-mb air. Only those that have discernable relationships with cloud properties are presented here.

1) GEOGRAPHICAL DISTRIBUTIONS

Figure 5 shows the spatial distributions of LTS (contours), surface air temperature advection (colors), and

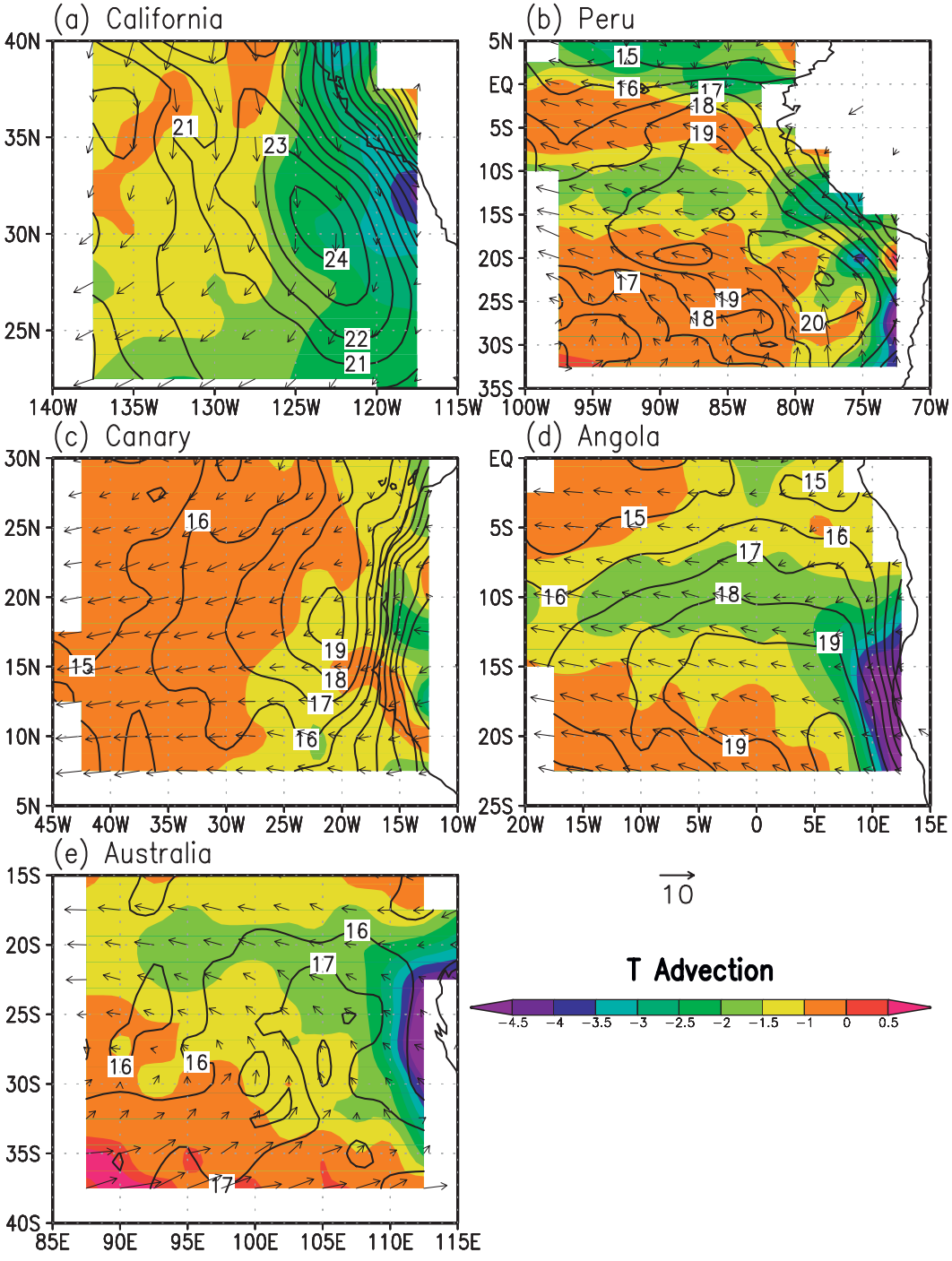

FIG. 5. Geographical distribution of meteorological properties for the five regions using the NCEP reanalysis collocated with cloud scenes. Shown are LTS (contours, K), advT (colors, K day^{-1}), and 850-mb circulation (vectors, m s^{-1}). LTS is defined as potential temperature difference between fixed levels at 700 and 1000 mb.

850-mb wind circulation (vectors) per region. These distributions are obtained by compositing over available cloud scenes, instead of simple temporal averages. Over each 2.5° × 2.5° grid, collocated meteorological parameters for all cloud scenes whose central points fall into the grid are used to obtain the median value for each field. The wind fields provide a synoptic setting for each of the MBL cloud regions, whereas LTS and temperature advection are important to CF, as will be seen later. Maximum LTS regions are oriented approximately parallel to

the coastlines in all five regions. The Californian region is the most stable, with maximum LTS reaching 24 K, whereas the Australian region is the least stable, with maximum LTS near 18 K. The surface air temperature advection is negative in all five regions, with coldest air advection near the coast and becoming gradually less so in the open ocean.

In California, weak cold air advection occurs in the west and northwest part of the region, where LTS is relatively low. The flow field is northerly in most of the region, turning to become northeasterly in the southern part of the domain. Over the Peruvian region, areas of high LTS correspond well with CF (see Fig. 2). The 850-mb wind is mostly from the southeast in the southern part of the domain, becoming easterly in the northern part, except north of the equator in the ITCZ region. In the Canarian region, highest LTS values are found near the coast. Although LTS tends to be large in areas of high CF, the largest LTS values are to the east of the maximum CF. The temperature advection is weak in most of the region, and the 850-mb wind is easterly and northeasterly in the entire domain. In the Angolan region, the high LTS region is located in areas of high CF. The cold air temperature advection has maxima along the coast south of 10°S and along the latitude belt centered near 10°S. This latter region is located just north of the high CF area. The 850-mb airflow is easterly to southeasterly in most of the domain, except in the northeastern corner, where it is northeasterly, blowing into the ITCZ near 10°S. Finally, the Australian region is characterized by nearly uniform LTS, with values varying in a small range around 16–17 K. Cold air advection occupies most of the domain, extending from the coast northwestward, except along the south boundary, where there is a slight warm advection. The wind field has a strong anticyclonic pattern; it is southwesterly in the south part and becomes southeasterly and easterly in the north.

In summary, comparison of the five MBL regions shows some common features shared by all five regions, which include the presence of cold air temperature advection and strong LTS. However, the strengths and the relationships among them vary from region to region. The Californian region has the largest LTS, followed by the Peruvian region; the Australian region has the smallest LTS. The cold air temperature advection is large in the Californian region and small in the Canarian region. All regions have offshore flow, except Australia, where the southern part of the region experiences onshore flow.

Before continuing, it is appropriate to compare our interregional LTS differences with those in previous work. Klein and Hartmann (1993) show that CF and LTS are highly correlated on seasonal to interannual time scales. Before we examine similar relationships with instantaneous observations, we note that some interregional LTS values in Fig. 5 are different from Klein and Hartmann. For example, in their work (their Fig. 13), the maximum seasonally averaged LTS values for Peru and Angola exceed that for California by about 1 K, and the Canarian region has the smallest LTS, varying from 14 to 16 K. However, in our analysis (Fig. 5), California has the largest LTS, which is greater than Peru and Angola by about 4 K, and the maximum for Peru is only about 1 K greater than for Canary. Several factors account for these seeming discrepancies. First, the regions used by Klein and Hartmann are much smaller than ours, and they are not centered on the regions where our LTS maxima are located for the Canarian and Californian regions (closer for the other three regions). Second, the composite geographic distribution in Fig. 5 considers only MBL-dominated cloud scenes. Therefore, the maps are weighted toward peak MBL cloud season in each region, whereas Klein and Hartmann take time averages within each season and all analysis times are thus weighted equally. Third, this study uses the current NCEP reanalysis product for LTS calculation, and Klein and Hartmann (1993) used the European Centre for Medium-Range Weather Forecasts (ECMWF) reanalysis product that was available 15 yr ago. Although it is difficult to know what the differences between the two reanalyses might be, an assessment of current versions was made by Stevens et al. (2007). They find that the NCEP reanalysis is warmer by 1.5 K at the 850-mb level than the ECMWF reanalysis at a field experiment site off the Californian coast in July 2001. Should the same be true at 700 mb for all other years and seasons (albeit a bold assumption), this would explain a difference of 1.5 K in LTS. Finally, although our Californian LTS values are distinctively greater than for Klein and Hartmann, we note that they compare very well with the more recent work by Lin et al. (2009).

2) CF RELATIONSHIPS TO METEOROLOGY

From a cloud parameterization point of view, one would want to know what the typical CF is given the meteorological conditions. Here, individual cloud scenes of size 300 km $\times$ 300 km for each region are binned according to meteorological parameters to examine the relationships between cloud coverage and meteorology, which, by considering the diverse regions together, provides a global-scale perspective. The binning procedure is as follows. For each region, the total number of cloud scenes over the 6-yr observation period (March 2000 through February 2006) is divided into eight equal portions after sorting by the meteorological parameter of interest (e.g., LTS). The median values of the meteorological parameter and CF for each bin are then determined and

plotted in Fig. 6, which shows CF as functions of LTS, advT, and LCL of surface air for each region. The LCL values calculated from the NCEP reanalysis were compared with those obtained by Lin et al. (2009) from the International Comprehensive Ocean–Atmosphere Dataset (ICOADS) in the California region, which were found to be generally in good agreement.

In all five regions, CF increases with LTS, slowly at first for LTS < 14 K and then almost linearly before slowing or leveling off at LTS > 19 K for Peru, Angola, and California. However, clear interregional differences are also seen, with the Peruvian and Angolan regions having the largest rate of increase and the Canarian region having the smallest. Such differences present a challenge to development of a cloud parameterization that treats all regions. Cloud fraction is also reasonably well related to surface cold air temperature advection, although the relationship is nonlinear. In general, CF increases with cold air temperature advection for intensities up to -2 to -3 K day^{-1}. Further increase in advection intensity corresponds to a decrease in CF for all regions. Although the general shapes of the relationships are similar for all regions, interregional differences are even more evident in the magnitudes of temperature advection. The regions with high CFs (California, Peru, and Angola) are in one group showing similar patterns, and the regions with low CFs (Australia and Canary) are in another group. The LCL, a measure of surface air humidity, is also well correlated with CF. About 88% of the cloud scenes (i.e., except the leftmost points, which account for 12.5% of the observations in each region) have LCL below the 930-mb height. Lower CF corresponds to drier surface air, and higher CF corresponds to moister surface air.

3) LWP AND DRIZZLE RELATIONSHIPS TO METEOROLOGY

As seen in Fig. 3, CF shows a shift toward smaller clouds (for the same CF) in the presence of drizzle. Although the shift is systematic, the overall impact on CF is small compared to the meteorological relationships (Fig. 6); therefore, it is not a dominant factor for determining CF. However, Jensen et al. (2008) found, consistent with other studies, that partitioning the cloud LWP by drizzle state has a strong signal, where drizzling clouds are associated with (possibly a result of) higher LWP than nondrizzling clouds, and therefore has important ramifications to the radiative energy budget. Thus, we investigate the relationships between meteorological state, cloud LWP, and drizzle frequency, which might be useful for GCM diagnostics.

Figure 7 shows the relationship between LWP and LTS. All regions but Canary show a general increase of

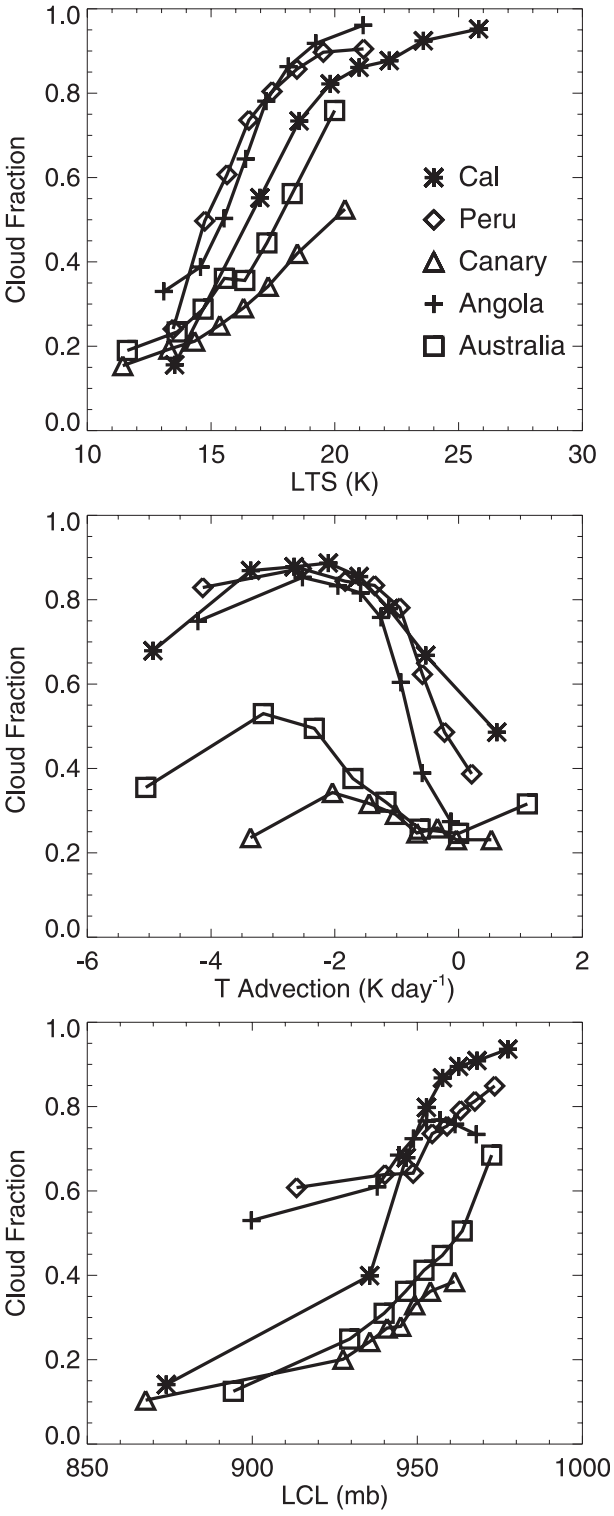

FIG. 6. CF binned as functions of (top) LTS, (middle) advT, and (bottom) LCL of surface air. The data for each region are divided into eight bins of equal numbers for each meteorological variable.

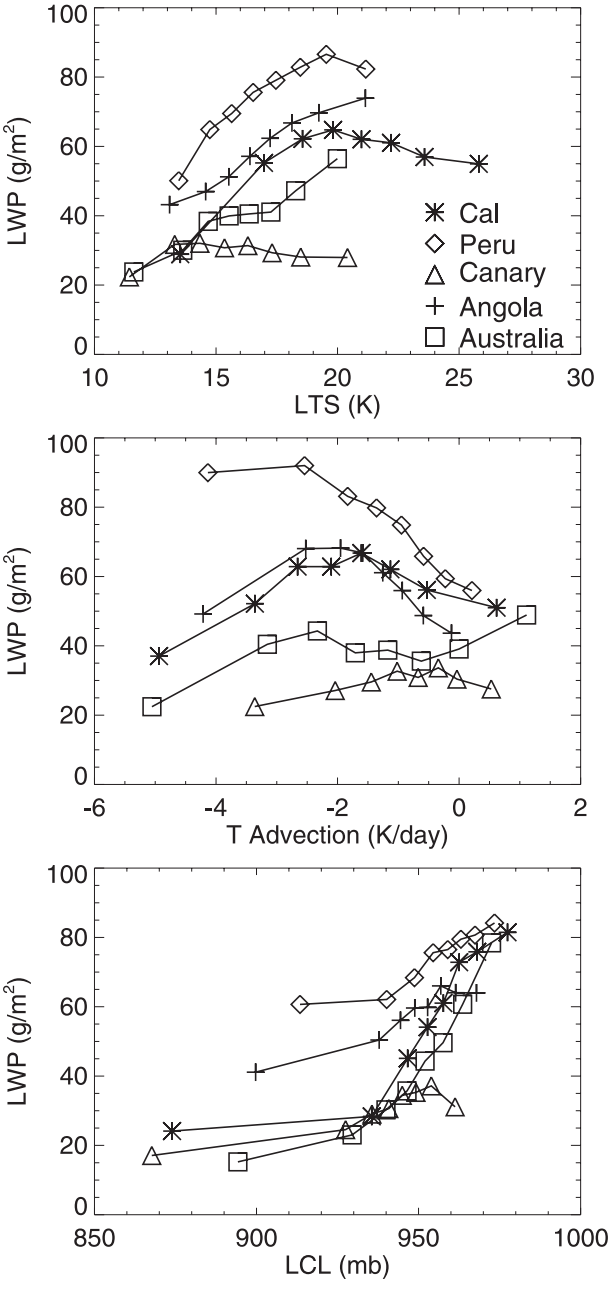

FIG. 7. Cloud LWP as a function of (top) LTS, (middle) advT, and (bottom) LCL.

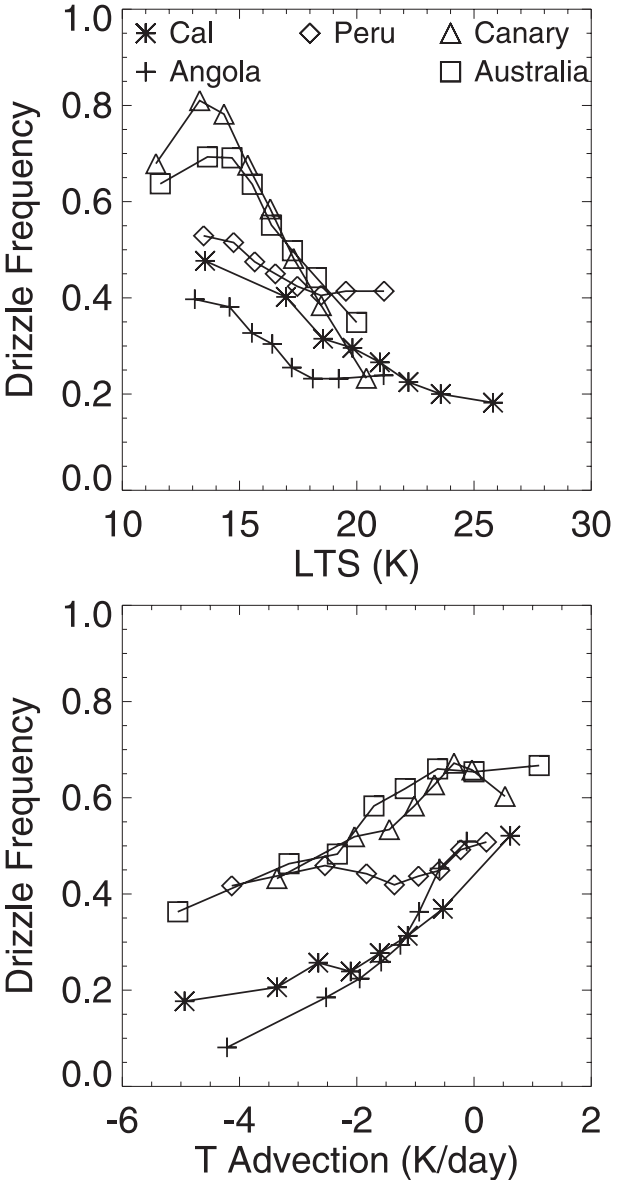

FIG. 8. Frequency of drizzle occurrence as a function of LTS and advT. Drizzling scenes are delimited by a cloud scene mean $r_e \geq 15$ μm. For each bin, the drizzle frequency is calculated as the number of drizzling scenes divided by the total number of scenes within that bin.

LWP with LTS, reaching maxima at LTS near 20 K. Further increase in LTS shows a slight decrease of LWP for regions having large LTS (e.g., California). The Canarian region LWP remains relatively flat, with changing LTS. Similar to CF, cloud LWP varies with cold temperature advection nonlinearly, peaking near the temperature advection of -2 to -3 K day^{-1} for most regions. As for the effect of the near-surface air moisture, almost without exception, moister air corresponds to larger LWP. It would be interesting to see if GCMs can simulate similar relationships between LWP, which is a cloud parameterization product, and meteorological state.

Jensen et al. (2008) show important seasonal regional variations in drizzle frequency; here, we find that drizzle frequency varies significantly with meteorological parameters as well. Despite large interregional differences (Fig. 8), drizzle frequency peaks in all regions at LTS near 13 K and decreases as LTS increase. For a given LTS, Canary and Australia have the highest drizzle

frequency, consistent with the lowest CF in these two regions as compared to other regions. Angola and California have the lowest drizzle frequency, again consistent with high CFs there. For temperature advection, drizzle frequency increases almost monotonically in all regions as the intensity of cold air advection decreases (trend weakest for Peru). This occurs despite the fact that the median CF in each bin varies very differently with temperature advection (Fig. 6), implying that the low CFs at weak cold air advection are more prone to drizzling than high CF at strong cold advection. We also examined the relationships between drizzle frequency and surface air LCL (not shown) and did not find them to be significant.

For clarity, we point out that the increase of LWP with LTS is not only influenced by the drizzle frequencies shown in Fig. 8 but also by the increase of LWP with CF. Figure 12 of Jensen et al. (2008) shows the strong correlation of LWP with cloud size (which correlates with CF) for both drizzling and nondrizzling clouds. Although, for a given cloud size, the drizzle frequency determines the weighting of the drizzle versus nondrizzle LWPs, changes in the cloud size (or, correlatively, CF) dominate the LWP difference. Because CF increases strongly with LTS (top of Fig. 6), it follows that LWP increases with LTS, as seen in Fig. 7.

In summary, in this section we find that LTS is the most useful meteorological parameter to relate to MBL CFs, with notable patterns also found for LCL and surface air temperature advection. Although this is not new, it confirms previous results from other observations. In addition, previous studies examined the relationship between CF and LTS on seasonal to interannual time scales and this study uses instantaneous cloud scenes, which are thus directly applicable to GCM cloud parameterization.

c. CF parameterization

1) Effective LTS

To facilitate the comparison of interregional differences, we have shown the median values of CF in each bin as functions of meteorological parameters for each region. For the purpose of providing a parameterization for GCM use, we combine the data to demonstrate the variation of CF on two meteorological parameters at a time (Fig. 9). We first investigate CF in terms of LCL and LTS (Fig. 9a). For a given LCL, CF increases with LTS; similarly, for a given LTS, CF generally increases with LCL. The role of temperature advection is nonlinear (Fig. 9b), which is consistent with Fig. 6. For warm advection (advT $>$ 0), CF has little dependence on temperature advection per LTS value. For $-3 <$ advT $<$ 0 K day^{-1}, CF increases with cold advection intensity

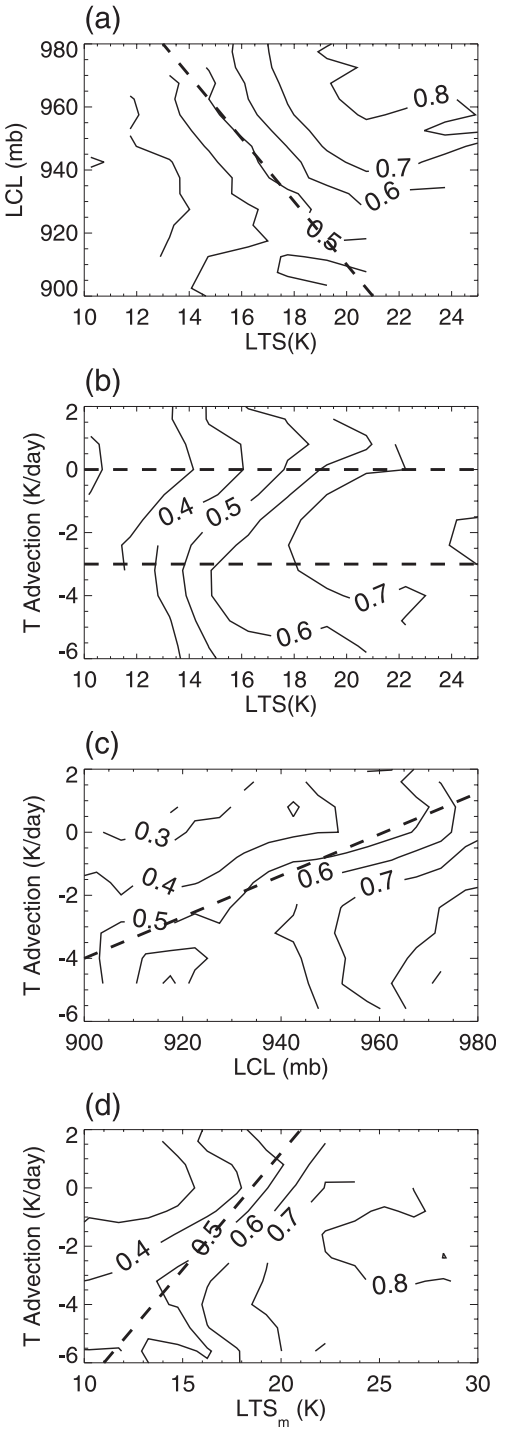

FIG. 9. Variation of CF with (a) LTS and LCL, (b) LTS and advT, (c) LCL and advT, and (d) LTS$_m$ and advT. See text for definition of LTS$_m$. Each meteorological variable is first divided into a number of bins; then, the CF within each bin grid is averaged and contoured. The dashed lines in (a),(c),(d) separate high and low CF regimes, which are discussed in the text and are used ultimately to define an eLTS. The dashed lines in (b) are at zero temperature advection, which separates warm from cold air advection, and at -3 K day^{-1}, which approximately corresponds to maximum cold air advection for a given LTS.

for all LTS values. For advT < -3 K day^{-1}, stronger cold advection leads to less cloud cover per LTS value. The variation of CF with temperature advection and LCL (Fig. 9c) shows that moist air (large LCL pressure) with cold air advection favors greater MBL CFs; conversely, dry air (low LCL pressure) with warm air advection favors low CF.

Note that, in a significant portion of the LTS–LCL space (Fig. 9a), CF contours have the largest gradient perpendicular to the dashed line shown, given by LCL = 980 − 10(LTS − 13), where LCL is in millibars and LTS is in kelvins. This implies that a combination of LTS and LCL could provide a better relationship to CF than either variable alone. To approximate in one variable the LCL and LTS dependence of CF, we define LTS_m as $\text{LTS}_m = \text{LTS} + (\text{LCL} - 980)/10 + 4.5$, where the subscript m denotes consideration of moisture effect on LTS and LTS_m is in kelvins (the addition of a constant makes the mean LTS_m value close to that of LTS for the observed cloud scene population). Through this linear combination, the CF information is contained predominately in LTS_m such that a contour plot of CF in terms of LCL and LTS_m (not shown) would have gradients only along the LTS_m axis.

The role of LCL on refining the relationship between CF and lower-tropospheric stability was first noted by Wood and Bretherton (2006). Through thermodynamic considerations, they defined an estimated inversion strength (EIS) as $\text{EIS} = \text{LTS} - \Gamma_m^{850}(z_{700} - z_{\text{LCL}})$, where Γ_m^{850} is the moist adiabatic potential temperature lapse rate and z_{700} and z_{LCL} are heights of the 700-mb pressure level and the lifting condensation level, respectively. They found that EIS was a better predictor of CF than LTS when compared to the seasonally averaged cloud observations of Klein and Hartmann (1993). However, when we applied EIS to individual cloud scenes in this study, no significant improvement over LTS was found.

In Fig. 9d, the covariation of advT and LTS_m are shown. Compared to Fig. 9b, use of LTS_m reduces some of the nonlinear dependence of CF on advT. However, the overall gradient does not lie in the direction of LTS_m. This reflects the effect of advT on CF, which is not incorporated in LTS_m. If a similar coordinate transformation is performed to consider the effect of temperature advection by using the dashed line in Fig. 9d as reference, we define an effective lower-tropospheric stability (eLTS) as

$$\text{eLTS} = \text{LTS} + 0.1(\text{LCL} - 980) - 1.25(\text{advT} - 2), \quad (4)$$

where eLTS and LTS are in kelvins, LCL is in millibars, and advT is in kelvins per day. Using eLTS, the dependence of CF on LTS, surface air moisture, and temperature advection are combined into a single parameter.

2) CF DEPENDENCE ON ELTS

To further understand the roles of LTS, eLTS, advT, and LCL in MBL clouds, Fig. 10 presents the frequency of occurrence of CF as functions of LTS (Figs. 10a–c) and eLTS (Figs. 10d–f). For LTS, the entire population of observations are plotted in Fig. 10a and then with the observations partitioned using the dashed line shown in Fig. 9a to delimit a dry air and low LTS regime (Fig. 10b) and a moist air and high LTS regime (Fig. 10c). The role of temperature advection is not addressed in this case. For eLTS, which is a combination of LTS, LCL, and advT, the entire population of observations is plotted in Fig. 10d and then with the observations partitioned using the dashed line shown in Fig. 9c to delimit a dry and warm air advection regime (Fig. 10e) and a moist and cold air advection regime (Fig. 10f). The median CFs for each LTS and eLTS bin are also plotted as filled circles connected with a solid line.

The most striking feature is the bimodal distribution of CF for both LTS and eLTS (Figs. 10a,d). For LTS $<$ 14 K, most of the observed CFs are below 20%; for LTS $>$ 19 K, most of the CFs are above 80%. However, in the intermediate range (LTS from 14 to 19 K), there is a similar likelihood that the CF is either very low, below 20%, or very high, above 80%. The same bimodality is exhibited when the regions are plotted separately (not shown). These ''competing maxima'' present an irresolvable ambiguity for a CF parameterization that is based solely on LTS. The median CF curve that results from these competing maxima varies nonlinearly with LTS and undergoes a steep rate of change for intermediate LTS as the curve shifts from one maximum to the other. For reference, the cloud fraction parameterization of Klein and Hartmann (1993) based on seasonally averaged data ($y = 0.057\text{LTS} - 0.5573$) is plotted in Fig. 10a as a dashed–dotted line. For instantaneous cloud scenes, the rate of change of cloud fraction with LTS from 15 to 24 K is significantly larger than predicted by the Klein and Hartmann parameterization.

Separation of observations into the categories of dry and low LTS (Fig. 10b) and moist and high LTS regimes (Fig. 10c) does not eliminate the bimodality in the frequency of occurrence for a given LTS, although distinct differences exist between the two groups. When LTS is less than 15 K, most of the observed cloud scenes are under the dry and low LTS condition. Similarly, for LTS greater than 18 K, most of the cloud scenes are under the moist and high LTS conditions. To enable comparing these two subsets, the median cloud fraction curve from Fig. 10b is overlaid in Fig. 10c. For the majority of observations, which fall within the 13 K $<$ LTS $<$ 22 K range, the moist and high LTS group (Fig. 10c) has

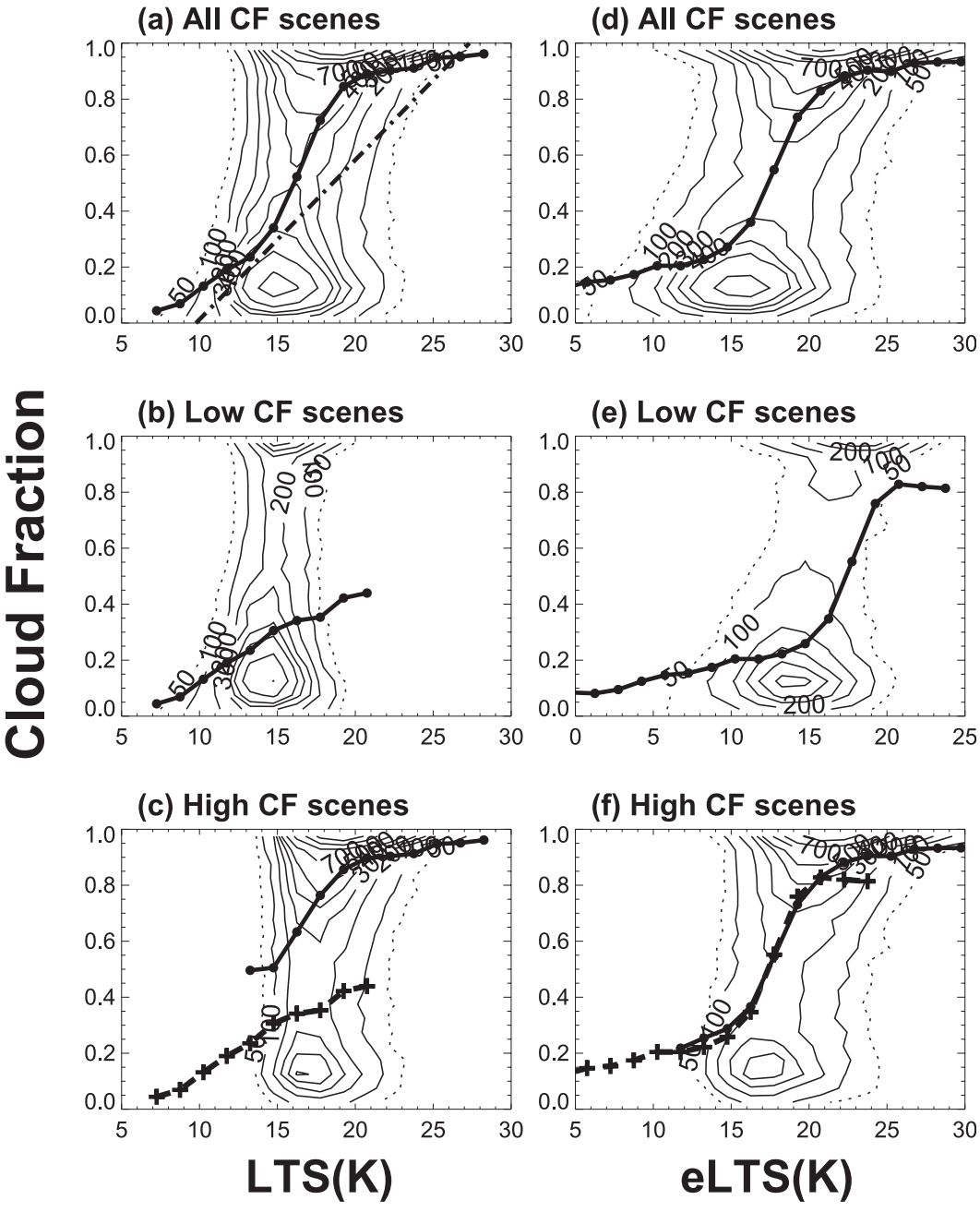

FIG. 10. Frequency of occurrence of CF varying with (a)–(c) LTS and (d)–(f) eLTS. The bin intervals are 0.05 (5%) for CF and 1.5 K for LTS and eLTS. The contour values are number of cloud scenes within each bin grid in intervals of 100, with contour value 50 shown as a thin dashed line. The median CF for each bin of LTS and eLTS is shown by the solid line with filled circles. The thick dashed–dotted line in (a) shows the relationship between CF and LTS from Klein and Hartmann (1993). Shown are (a),(d) the entire cloud scene observations; (b),(c) two mutually exclusive subsets of (a) separated by the dashed line in Fig. 9a; and (e),(f) subsets of (d) separated by the dashed line in Fig. 9c. The median curves in (b),(e) are superposed in (c),(f), respectively, as dashed lines for reference.

significantly larger median cloud fractions than the dry and low LTS group (Fig. 10b) for the same LTS values. At least part of this difference may be due to the effect of temperature advection.

The use of eLTS (Fig. 10d) improves moderately over LTS (Fig. 10a) for the separation of low and high MBL cloud fraction regimes, as shown by the slight tilt of contours in eLTS compared to the more vertical contours

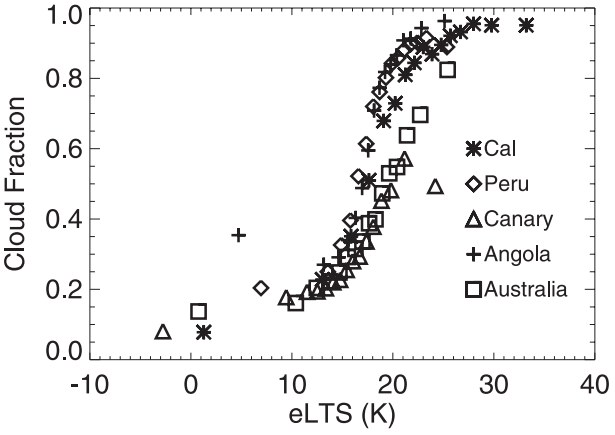

FIG. 11. As in Fig. 6 (top), but using eLTS instead of LTS.

in LTS space. When temperature advection is considered (Figs. 10e,f), the bimodality is reduced more for eLTS than for LTS, as indicated by the much larger separation in the frequency of occurrence maxima in eLTS values than in LTS values (Figs. 10e,f versus Figs. 10b,c). The separations between the median cloud fractions in Figs. 10e,f are manifestations of the effect of temperature advection regimes. Contrary to the LTS result, the two median curves virtually overlap each other for their common eLTS values, which indicates that eLTS indeed maximizes the separation of CF information.

As a further test of the usefulness of eLTS, we repeated the calculation used for the top plot in Fig. 6, except replacing LTS with eLTS, as defined in Eq. (4). Figure 11 shows median CF in each bin as functions of eLTS for each of the five regions. Excepting two points, all regions largely collapse into a curve, as compared to a wide interregional spread shown in Fig. 6 (exceptions are an Angolan point at an eLTS of 5 K and a Canarian point at 24 K). This shows that eLTS is a powerful parameter that has the potential to provide an improved, unified MBL cloud parameterization.

3) CF PARAMETERIZATION AND ASSESSMENT

For parameterization purposes, we use the relationship between eLTS and CF as shown by the median values in Fig. 10d to parameterize CF. A sigmoid fit to the CF dependence on eLTS in Fig. 10d yields the following equation:

$$\mathrm{CF} = a_0 + \frac{a_1}{(1 + e^{a_2 x + a_3})} + \frac{a_4}{(1 + e^{a_5 x + a_6})}, \qquad (5)$$

where x is eLTS and the fitting coefficients a_0–a_6 are 0.02, 0.46, −0.13, 1.9, 0.52, −0.96, and 17, respectively. The fit is valid for $-10 < \mathrm{eLTS} < 30$ and is visually indistinguishable from the median value curve if plotted in Fig. 10d, with an average fitting error in CF of 0.0005.

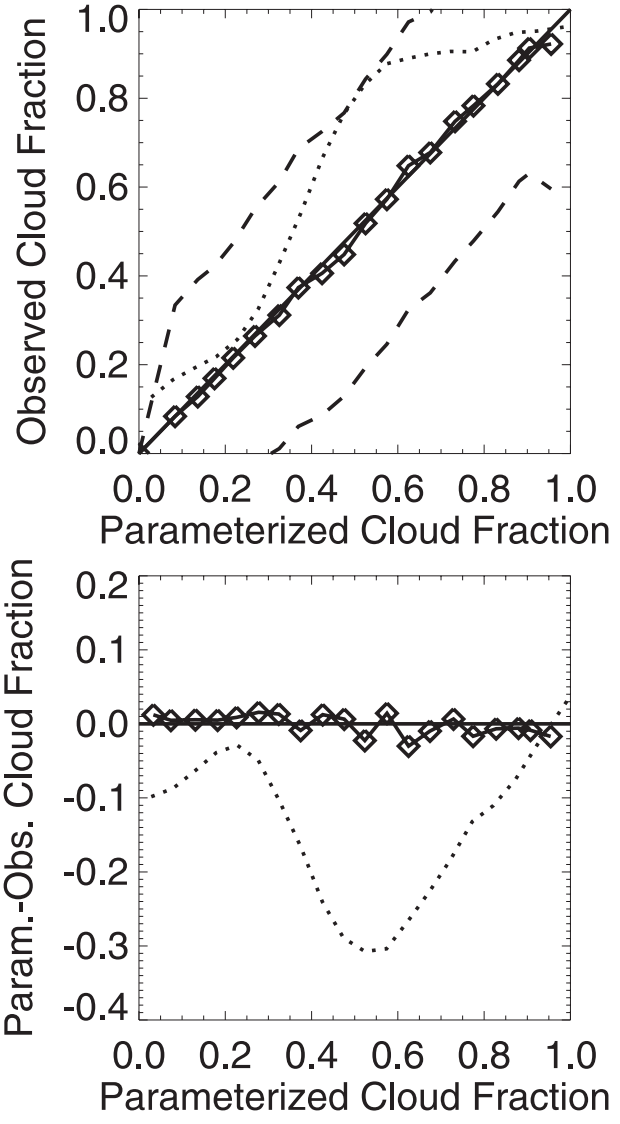

FIG. 12. (top) Observed vs parameterized CF (diamonds) based on the fitting of the median curve of CF vs eLTS in Eq. (5) and shown in Fig. 10d. The dashed lines show the standard deviation, and the solid diagonal line is the 1:1 reference. The dotted line uses Klein and Hartmann's LTS relationship. (bottom) The differences between parameterized and observed CFs using Eq. (5) and Klein and Hartman's equation are shown.

Figure 12 compares the observed CF with the parameterized CF obtained for eLTS. The procedure of the comparison is as follows: For each observed cloud scene, there is a collocated eLTS calculated from Eq. (4). A parameterized CF is obtained using this eLTS and Eq. (5). These parameterized CF values are then binned into 0.05 (or 5%) intervals, and the corresponding observed CFs within each bin are used to obtain the median value. The standard deviation for each bin is also plotted for reference. The same procedure is repeated using the

Klein and Hartmann (1993) parameterization and is shown in Fig. 12, where only the median is plotted. The parameterized CF and the observations agree very well. However, the standard deviation is large, reflecting the fact that the frequency of occurrence distribution (Fig. 10d) still has a large spread from the median, despite the use of eLTS. The Klein and Hartmann parameterization shows a large underestimation, by as much as 0.3. This result is consistent with the underestimation of MBL CF, based on the Klein and Hartmann parameterization, that was found in the NCAR Community Climate System Model (Dai and Trenberth 2004). They show that, even using the NCEP reanalysis LTS, it still underestimated the observed cloud cover.

The large standard deviation shown in Fig. 12 is rather troublesome. Although statistically the parameterization will produce the right cloud amount when averaging over many cases within similar eLTS regimes, it does not replicate the variability. Likewise, for different eLTS regimes, the same CF may be observed (cf. Fig. 10), but the parameterization will predict a range of CFs. The large standard deviation in Fig. 12 is a direct consequence of the mismatch between the median value and the frequency of occurrence maxima in Fig. 10d. For instance, at an eLTS of 18 K, the observed median CF is 0.5 (as is the parameterized CF). However, the occurrence frequency is a minimum: that is, the predicted CF is least likely to occur and has little bearing on the most probable CF values that can be either high (above 0.8) or low (below 0.2). However, averaging over the long term should give reasonable estimates of the observed cloud climatology (provided that underpredicting the variability does not induce feedbacks that push the simulated meteorological state significantly away from that observed). An alternative that would at least attempt to address the mismatched variability would be to use the frequency of occurrence distribution to predict the likelihood of the occurrence of a given CF statistically, rather than using the median value curve to predict CF deterministically. Such an approach, however, would require additional research that is beyond the scope of this paper.

4. Summary

This study documents the distribution of 6 yr of cloud properties observed by MODIS on board the NASA *Terra* satellite for five marine boundary layer cloud regions and analyzes their relationships to the prevailing meteorological conditions using near-surface meteorological parameters from collocated NCEP reanalysis data. The cloud properties addressed are cloud fraction (CF), effective cloud diameter C_D, liquid water path (LWP), and scene-wide drizzle state. All five regions have significant amounts of low-level cloud, with the largest CFs occurring in the Californian region and the smallest occurring in the Canarian region. A new parameterization is provided that relates CF to C_D [Eq. (3)], similarly to Jensen et al. (2008), but expands its applicability to include all CFs (versus having a 20% lower limit). It is used to show that drizzling clouds tend to be smaller for the same CF, which is consistent with the observations that open cells are associated with drizzle (Comstock et al. 2007).

From a meteorological perspective, all regions are associated with a stable lower troposphere and surface cold air advection. The regions generally experience offshore flow, except the Australian region that has an onshore flow for the southern half of the domain. Although the multiple regions have similar meteorological values, they also exhibit striking differences (Fig. 5). For example, the Californian region stands alone as having the strongest LTS (by 4 K). From a GCM cloud parameterization point of view, cloud properties must be represented in terms of meteorological properties computed by the models at each time step. This study shows that, using instantaneous cloud scenes and the NCEP reanalysis data, CF depends strongly on variations in LTS and to a lesser extent on surface air temperature advection and lifting condensation level (Fig. 6). The dependence of LWP and drizzle-occurrence frequency on near-surface meteorology is also examined. LWP generally increases with LTS and then plateaus at LTS $\sim$ 20 K, and moister surface air corresponds to larger LWP (Fig. 7). Cloud drizzle frequency strongly depends on the meteorological conditions (Fig. 8). Weaker LTS and near-zero cold air advection favor drizzle, whereas the converse hinders drizzle (e.g., strong LTS and strong cold air advection). With the large regional differences shown in Figs. 7 and 8 between the meteorological state and the cloud LWP and drizzle frequency, such relationships might be useful for GCM diagnostic testing.

Overall, the meteorological properties combine to provide a wide variety of states with similar cloud cover values (or vice versa; Fig. 6), which presents a challenge to capture in a single, unified MBL cloud representation. The general functional shapes of the relationships are similar among the regions per variable, although their magnitudes can differ significantly. The similarity of the functions is encouraging to development of a CF parameterization, should the differences in the magnitudes be managed. We propose the use of eLTS [defined in Eq. (4)], which attempts to incorporate, in a single variable, the effects on CF of LTS, LCL, and surface air temperature advection. Results indicate that eLTS offers a marked improvement over LTS alone in explaining

the mean CF variations within the different study regions (Fig. 6 versus Fig. 11) and better separates the competing maxima that are found in frequency of occurrence plots of CF (Fig. 10). A parameterization of CF in terms of eLTS [Eq. (5)] produces results that improve over the Klein and Hartmann LTS-only parameterization. The median values from our parameterization differ negligibly from observations, whereas the LTS-only representation underestimates CF typically by 0.1–0.3 (Fig. 12).

However, the eLTS parameterization does not account well for the variability, as seen by the large standard deviations for all CF values in Fig. 12. Averaging over a long term should give reasonable estimates of the observed cloud climatology. However, we suggest an alternative approach that would at least attempt to address the unresolved or mismatched variability. The approach would use the frequency of occurrence distributions (Fig. 10) to predict the likelihood of the occurrence of a given CF statistically, rather than using the median value curve [Eq. (5)] to predict CF deterministically. However, developing and testing such an approach would require additional research that is beyond the scope of this paper.

Because aerosol observations are not included in our analysis, they may contribute to the unexplained variability in Figs. 10 and 12. Aerosol–cloud interactions are known to play a role in MBL cloud microphysics and are likely embedded within our cloud observations, particularly in seasons and areas associated with persistent aerosol loading (e.g., near the coastlines). For example, research suggests that POC formation can occur within mere days (Wood et al. 2008) and may be related to the precipitation activation by aerosol (Sharon et al. 2006; Petters et al. 2006; Rosenfeld et al. 2006), because the occurrence of drizzle may play a key role in forming and sustaining the observed cellular structures (Wood et al. 2008).

The meteorological properties used to compute eLTS are large scale and change gradually, which seem consistent with the seasonal to annual time scales observed to dominate MBL cloud variability (Rozendaal and Rossow 2003). Interestingly, Wood and Hartmann (2006) found that the type of MCC is not very sensitive to the large-scale meteorological state, which implies that other factors (aerosol–precipitation relationships) dominate the cellular development that can occur rapidly (e.g., Wood et al. 2008). Such processes might contribute to the daily to monthly time-scale variability, which Rozendaal and Rossow (2003) found to have a nonnegligible but smaller impact than for the seasonal to annual time scales. Thus, to the first order, the parameterization problem might be simplified by separation into one of a large-scale treatment, such as using eLTS to explain the slower variation of the cloud occurrence, upon which is superimposed the aerosol and precipitation events (POCs) to explain the important short-term variations. Further work will be needed to explore the relationships between these cloud properties, the aerosol properties, and the representation of the associated radiative effect in global climate models.

Acknowledgments. This work was supported by GWEC Grant NASA NAG5-11716, the Office of Science Biological and Environmental Research Program (BER), U.S. Department of Energy Grant DE-FG02-09ER64736, the NSF Grant ATM-0832915, and the Brookhaven National Laboratory. Collins's work was supported by the Director, Office of Science of the U.S. Department of Energy under Contract DE-AC02-05CH11231.

REFERENCES

Bender, F. A.-M., H. Rodhe, R. J. Charlson, A. M. L. Ekman, and N. Loeb, 2006: 22 views of the global albedo—Comparison between 20 GCMs and two satellites. *Tellus,* **58A,** 320–330, doi:10.1111/j.1600-0870.2006.00181.x.

Bennartz, R., 2007: Global assessment of marine boundary layer cloud droplet number concentration from satellite. *J. Geophys. Res.,* **112,** D02201, doi:10.1029/2006JD007547.

Collins, W. D., and Coauthors, 2004: Description of the NCAR Community Atmosphere Model (CAM3.0). NCAR Tech. Note NCAR/TN-464+STR, 214 pp.

Comstock, K. K., C. S. Bretherton, and S. E. Yuter, 2005: Mesoscale variability and drizzle in southeast Pacific stratocumulus. *J. Atmos. Sci.,* **62,** 3792–3807.

——, S. E. Yuter, R. Wood, and C. S. Bretherton, 2007: The three dimensional structure and kinematics of drizzling stratocumulus. *Mon. Wea. Rev.,* **135,** 3767–3784.

Dai, A., and K. E. Trenberth, 2004: The diurnal cycle and its depiction in the Community Climate System Model. *J. Climate,* **17,** 930–951.

Jensen, M. P., A. M. Vogelmann, W. D. Collins, G. J. Zhang, and E. P. Luke, 2008: Investigation of regional and seasonal variations in marine boundary layer cloud properties from MODIS observations. *J. Climate,* **21,** 4955–4973.

King, M. D., and Coauthors, 2003: Cloud and aerosol and water vapor properties, percipitable water, and profiles of temperature and humidity from MODIS. *IEEE Trans. Geosci. Remote Sens.,* **41,** 442–458.

Kistler, R., and Coauthors, 2001: The NCEP–NCAR 50-Year Reanalysis: Monthly means CD-ROM and documentation. *Bull. Amer. Meteor. Soc.,* **82,** 247–267.

Klein, S. A., and D. L. Hartmann, 1993: The seasonal cycle of low stratiform clouds. *J. Climate,* **6,** 1587–1606.

——, ——, and J. R. Norris, 1995: On the relationships among low cloud structure, sea surface temperature, and atmospheric circulation in the summertime northeast Pacific. *J. Climate,* **8,** 1140–1155.

Lin, W., M. Zhang, and N. G. Loeb, 2009: Seasonal variation of the physical properties of marine boundary layer clouds off the California coast. *J. Climate,* **22,** 2624–2638.

Ma, C. C., C. R. Mechoso, A. W. Robertson, and A. Arakawa, 1996: Peruvian stratus clouds and the tropical Pacific circulation: A coupled ocean–atmosphere study. *J. Climate,* **9,** 1635–1645.

Masunaga, H., T. Y. Nakajima, T. Nakajima, M. Kachi, and K. Suzuki, 2002: Physical properties of maritime low clouds as retrieved by combined use of Tropical Rainfall Measuring Mission (TRMM) Microwave Imager and Visible/Infrared Scanner 2. Climatology of warm clouds and rain. *J. Geophys. Res.,* **107,** 4367, doi:10.1029/2001JD001269.

Mochizuki, T., T. Miyama, and T. Awaji, 2007: A simple diagnostic calculation of marine stratocumulus cloud cover for use in general circulation models. *J. Geophys. Res.,* **112,** D06113, doi:10.1029/2006JD007223.

Norris, J. R., and C. B. Leovy, 1994: Interannual variability in stratus cloudiness and sea surface temperature. *J. Climate,* **7,** 1915–1925.

Petters, M. D., J. R. Snider, B. Stevens, G. Vali, I. Faloona, and L. M. Russell, 2006: Accumulation mode aerosol, pockets of open cells, and particle nucleation in the remote subtropical Pacific marine boundary layer. *J. Geophys. Res.,* **111,** D02206, doi:10.1029/2004JD005694.

Philander, S. G. H., D. Gu, D. Halpern, G. Lambert, N.-C. Lau, T. Li, and R. C. Pacanowski, 1996: Why the ITCZ is mostly north of the equator. *J. Climate,* **9,** 2958–2972.

Pinsky, M. B., and A. P. Khain, 2002: Effects of in-cloud nucleation and turbulence on droplet spectrum formation in cumulus clouds. *Quart. J. Roy. Meteor. Soc.,* **128,** 501–534.

Platnick, S., M. D. King, S. A. Ackerman, W. P. Menzel, B. A. Baum, J. C. Riedi, and R. A. Frey, 2003: The MODIS cloud products: Algorithms and examples from *Terra*. *IEEE Trans. Geosci. Remote Sens.,* **41,** 459–473.

Rosenfeld, D., Y. J. Kaufman, and I. Koren, 2006: Switching cloud cover and dynamical regimes from open to closed Benard cells in response to the suppression of precipitation by aerosols. *Atmos. Chem. Phys.,* **6,** 2503–2511.

Rozendaal, M. A., and W. B. Rossow, 2003: Characterizing some of the influences of the general circulation on subtropical marine boundary layer clouds. *J. Atmos. Sci.,* **60,** 711–728.

Shao, H., and G. Liu, 2004: Detecting drizzle in marine warm clouds using combined visible, infrared, and microwave satellite data. *J. Geophys. Res.,* **109,** D07205, doi:10.1029/2003JD004286.

Sharon, T. M., B. A. Albrecht, H. H. Jonsson, P. Minnis, M. M. Khaiyer, T. M. van Reken, J. Seinfeld, and R. Flagan, 2006: Aerosol and cloud microphysical characteristics of rifts and gradients in maritime stratocumulus clouds. *J. Atmos. Sci.,* **63,** 983–997.

Siebesma, A. P., and Coauthors, 2004: Cloud representation in general-circulation models over the northern Pacific Ocean: A EUROCS intercomparison study. *Quart. J. Roy. Meteor. Soc.,* **130,** 3245–3267.

Stevens, B., G. Vali, K. Comstock, R. Wood, M. C. van Zanten, P. H. Austin, C. S. Bretherton, and D. H. Lenschow, 2005: Pockets of open cells and drizzle in marine stratocumulus. *Bull. Amer. Meteor. Soc.,* **86,** 51–57.

——, A. Beljaars, S. Bordoni, C. Holloway, M. Köhler, S. Krueger, V. Savic-Jovcic, and Y. Zhang, 2007: On the structure of the lower troposphere in the summertime stratocumulus regime of the northeast Pacific. *Mon. Wea. Rev.,* **135,** 985–1005.

Wood, R., and C. S. Bretherton, 2006: On the relationship between stratiform low cloud cover and lower-tropospheric stability. *J. Climate,* **19,** 6425–6432.

——, and D. L. Hartmann, 2006: Spatial variability of liquid water path in marine low cloud: The importance of mesoscale cellular convection. *J. Climate,* **19,** 1748–1764.

——, K. K. Comstock, C. S. Bretherton, C. Cornish, J. Tomlinson, D. R. Collins, and C. Fairall, 2008: Open cellular structure in marine stratocumulus sheets. *J. Geophys. Res.,* **113,** D12207, doi:10.1029/2007JD009371.

Wylie, D., B. B. Hinton, and K. Kloesel, 1989: The relationship of marine stratus clouds to wind and temperature advection. *Mon. Wea. Rev.,* **117,** 2620–2625.

Xu, H., S.-P. Xie, and Y. Wang, 2005: Subseasonal variability of the southeast Pacific stratus cloud deck. *J. Climate,* **18,** 131–142.

Zhang, M. H., and Coauthors, 2005: Comparing clouds and their seasonal variations in 10 atmospheric general circulation models with satellite measurements. *J. Geophys. Res.,* **110,** D15S02, doi:10.1029/2004JD005021.